Article

Casimir Forces with Periodic Structures: Abrikosov Flux Lattices

Shunashi G. Castillo-López , Raúl Esquivel-Sirvent , Giuseppe Pirruccio , Carlos Villarreal *

Posted Date: 6 December 2023

doi: 10.20944/preprints202312.0293.v1

Keywords: casimir; superconductor; fluxon; Abrikosov lattice, vortex

Article

Casimir Forces with Periodic Structures: Abrikosov Flux Lattices

Shunashi Castillo-López, Raúl Esquivel-Sirvent, Giuseppe Pirruccio and Carlos Villarreal *

Instituto de Física, Universidad Nacional Autónoma de México, Apdo. Postal 20-364, CDMX 01000, Mexico
* carlos@fisica.unam.mx
† All authors contributed equally to this work.

Abstract: We investigate the influence of the Abrikosov vortex lattice on the Casimir force in a setup constituted by high-temperature superconductors subject to an external magnetic field. The Abrikosov lattice is a property of type II superconductors in which normal and superconducting carriers coexist and these latter define a periodic pattern with squared symmetry. We find that the optical properties determined by spatial redistribution of the superconducting order parameter induce Casimir forces with a periodic structure whose minimal strengths coincide with the vortex cores.

Keywords: Casimir; superconductor; fluxon; Abrikosov lattice; vortex

1. Introduction

Seventy-five years have passed since, motivated by a suggestion by Bohr during a walk, HBG Casimir proposed that vacuum fluctuations could induce an attractive force per unit area between two perfectly conducting parallel plates, a distance d apart, given by $F = \hbar c/240d^4$ [1]. A more realistic theory was proposed by Lifshitz in 1956 by considering fluctuating electrodynamics, subtended on the fluctuation-dissipation mechanism. Lifshitz theory allows to determine the Casimir force in terms of the dispersive and dissipative properties of the materials [2], as described by its optical properties. Grounded on Lifshitz formulation, numerous experiments [3–13] have been performed on measuring the Casimir forces involving a diversity of experimental arrangements and materials [14–17]. The influence and taming of these forces in the design and construction of micro- and nanodevices is a current field of research.

In spite of the fruitful advances in the investigations of the Casimir effect there exist yet pending fundamental problems on the basic theory, concerning the role of dissipative mechanisms on the strength of the force between metallic bodies. In principle, the inclusion of this kind of contributions in the theoretical characterization of the optical response of materials involved in a given setup should be necessary to achieve formal congruence with the fluctuation-dissipation theorem lying on the grounds of Lifshitz theory. However, different measurements of Casimir forces in metals at room temperature at body separations $d \sim 50 - 600$ nm show consistence with theoretical predictions if dissipative effects are neglected. On the contrary, experiments carried out at larger separations $d \sim 700$ nm, such that $k_B T \sim \hbar c/d$, display a better agreement with predictions including electronic relaxation.

It has been proposed that the study of the Casimir effect in superconducting (SC) materials may constitute an excellent scenario to asses the influence of relaxation phenomena on the strength of the Casimir force between metallic bodies [18–22]. This is motivated by the fact that charge carriers in these materials exhibit a transition from dissipative transport to a dissipationless coherent behavior at a critical temperature $T = T_c$, However, measurements of the influence of the SC transition on the Casimir force in setups involving conventional BCS superconductors turn out to be extremely difficult, since for typical values $T_c \sim 1$ K, and $k_B T_c \ll \hbar c/d$ for sub-μm body separations. Therefore, indirect approaches have been proposed based on observations of the Casimir-induced shift of the critical magnetic field H_c of a thin superconducting film, or differential measurements of the Casimir force [23,24].

Preprints (www.preprints.org) | NOT PEER-REVIEWED | Posted: 6 December 2023 doi:10.20944/preprints202312.0293.v1

This suggests that the use of high-temperature superconductors (HTSCs), with $T_c \approx 100$ K, could constitute a suitable alternative to perform a direct analysis of the effect of the SC transition on the Casimir effect. In previous works, we investigated the Casimir forces between objects made of optimally doped $YBa_2Cu_3O_{7-\delta}$ (YBCO), with $T_c = 93$ K , either in thermal [25], or out of thermal equilibrium [26]. In the first case, we found that the Casimir force displays an abrupt increment as the $T \to T_c$, for temperatures $T > T_c$. On the other hand, for $T < T_c$, the force acquires an asymptotic behavior $\sim 1/d$ in the limit $T \ll T_c$. In the second case, each slab was in local equilibrium with a thermal reservoir at respective temperatures, $T_1 = 300$ K and T_2, where $300 \geq T_2 \geq 0$ K. In contrast with the thermal equilibrium situation, the Casimir force displays an abrupt decrement in the transit from normal metal to the SC state as $T_2 \to T_c$. The low-temperature asymptotic behavior of the force is similar to that displayed in the equilibrium situation.

To get further insight on the influence of superconductivity-related effects on the Casimir effect, in this work we study the effect of the Abrikosov lattice (AL) [27] on the local properties of Casimir forces associated to HTSCs. The AL is a manifestation of the Meissner effect, in which the presence of an external magnetic field induces surface screening supercurrents, which expel out the magnetic field lines from the material's interior within a London penetration length $\lambda_L(T) \sim n_s(T)^{-1/2}$. Here, $n_s(T)$ is the number density of Cooper pairs (CPs) at a temperature T. In the case of type-II superconductors, like YBCO, the Meissner effect involves the existence of a mixed phase of coexistence of normal and SC charge carriers determined by two critical fields, $\mathbf{H}_{c1} < \mathbf{H}_{c2}$. For values of the applied field higher than $\mathbf{H}_{c1}$, magnetic flux lines penetrate the sample in the form of quantum vortexes, with an intensity $\Phi_0 = h/2e$, thus inducing local screening currents to overcome the applied field [28]. Upon increasing magnitude of the field, the vortex density increases and saturates at the upper critical field $\mathbf{H}_{c2}$, where superconductivity disappears. Remarkably, as shown by Abrikosov [27], for intensities of the applied field just below H_{c2} the vortexes align in a compact square lattice with period $L_x = L_y = \sqrt{2\pi}\xi(T)$, where $\xi(T)$ is the CP coherence length. In the case of YBCO, $\xi(0) \equiv \xi_0 \approx 1.65$ nm, while $\lambda_L(0) \equiv \lambda_0 \approx 156$ nm, while the temperature-independent ratio $\kappa = \lambda_L(T)/\xi(T) \approx 95$ [28].

It can be shown that the AL vortexes strongly repel each other, giving rise to highly correlated configurations which are stable when thermal fluctuations and disorder are both negligible. A measure of the magnitude of the energy associated to thermal fluctuations with respect to the magnetic condensation energy is provided by the Ginzburg number, G_i, given by

$$Gi = 4\pi^2\gamma \left(\frac{\lambda_0^2}{\xi_0^2}\right) \frac{k_B T_c}{\Phi_0^2}, \tag{1}$$

where γ is a measure of the conducting anisotropy. In the case of conventional BCS superconductors $Gi = 10^{-7}$. In comparison, in the case of HTSCs, $T_c \sim 10^2$ K and $\kappa \sim 10^2$, implying that $G_i \sim 10^{-2}$. This relatively large value of G_i joined with the fact that these materials display a layered anisotropic structure at the atomic level, conduces to the manifestation of a manifold of phenomena generally termed as vortex matter, encompassing a complex phase diagram under different environmental conditions and material compositions [29]. Thus, thermal fluctuations may significantly alter the properties of the AL, generally leading to melting towards a liquid phase displaying vortex deformation, entanglement or migration. Superposed with repulsive interactions and thermal fluctuations, disorder due to material imperfections induce vortex pinning, which may conduce to the formation of glassy configurations [29–31]. Vortex matter has been investigated by recurring to techniques such as scanning tunneling microscopy [32] or muon spin rotation [33], among others.

In order to examine the influence of the AL on the Casimir force, in this work we consider a setup, depicted in Figure 1, constituted by a spherical Au nanoparticle located at a minimum distance d from a planar YBCO substrate, in presence of an applied magnetic field directed along the z axis. We show

Preprints (www.preprints.org) | NOT PEER-REVIEWED | Posted: 6 December 2023 doi:10.20944/preprints202312.0293.v1

that the force acquires a spatial structure congruent with the AL due to the modulation imprinted by the vortexes on the dielectric permittivity.

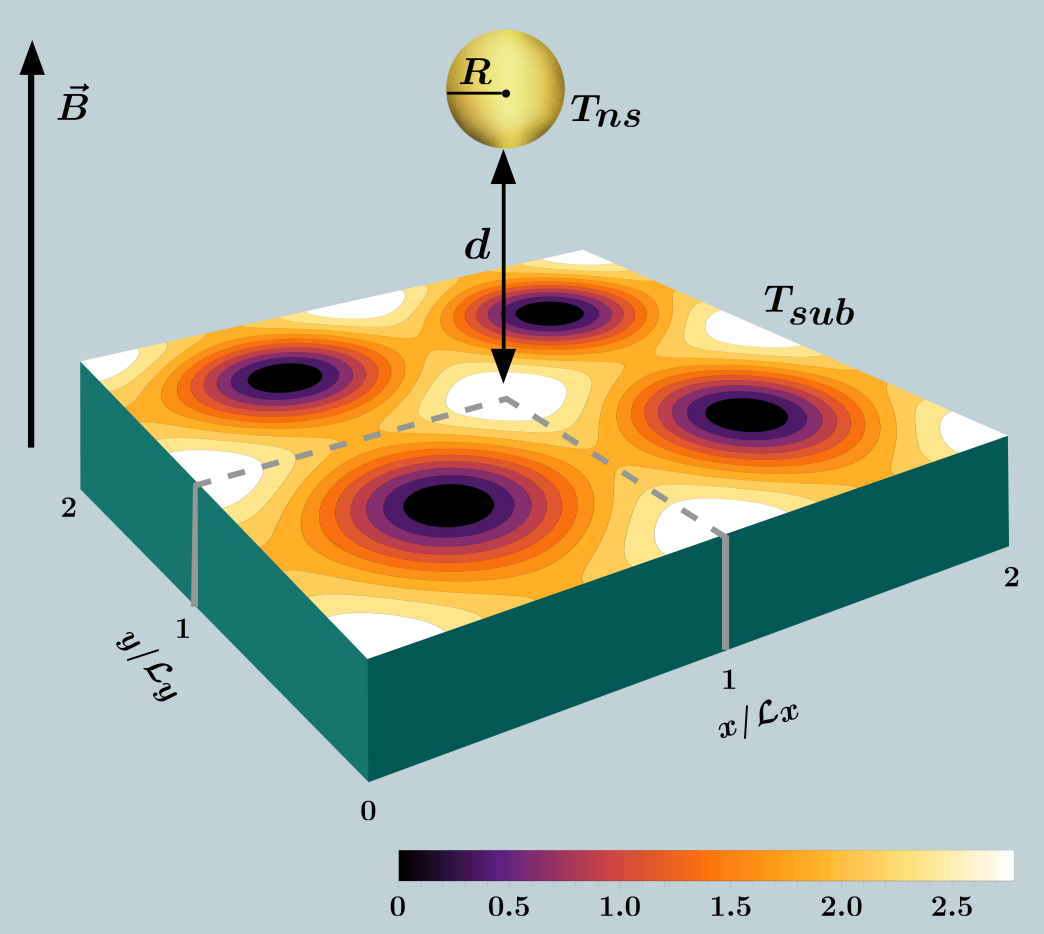

Figure 1. Setup consisting of a spherical Au nanoparticle of radius R located at a minimum distance d from a planar substrate made of optimally-doped YBCO, in presence of an applied magnetic field directed along the z axis. We show the resulting lattice structure with elementary cells of spatial periods $a = \mathcal{L}_x = \mathcal{L}_y = \sqrt{2\pi}/\kappa$. Induced supercurrents coincide with equiprobability contours defined by $n_s = |\Psi(\tilde{\mathbf{r}})|^2$. The vortex cores of radius ξ correspond to the darkest inner zones.

In the following, we present the formalism aimed to evaluate the Casimir force between a planar substrate and a nanosphere, which relies upon the frequency-dependent optical properties of the involved materials. To investigate the optical response of YBCO under the action of an external magnetic field, we then discuss a generalization of the Ginzburg-Landau (GL) theory of superconductivity, which allows the consideration of the anisotropic properties HTSCs, allowing the characterization of the spatial-dependent density of SC pairs, $n_s(\mathbf{r})$, in presence of an external magnetic field, as provided by the Abrikosov solution of the GL equation. We then discuss the thermal behavior of $n_s(\mathbf{r})$ by taking into account that SC charge carriers in HTSCs may be described as a 2D gas of weakly-interacting CPs able to form a Bose-Einstein condensate (BEC). In the following section, we model the optical response of YBCO by combining the derived expression for $n_s(\mathbf{r}, T)$ with experimental data for the YBCO dielectric function obtained in the normal ($T = 100$ K) and SC regime ($T = 2$ K). We then integrate the former antecedents to evaluate the Casimir force associated to the AL, and discuss the derived results.

Preprints (www.preprints.org) | NOT PEER-REVIEWED | Posted: 6 December 2023 doi:10.20944/preprints202312.0293.v1

2. Materials and Methods

2.1. Casimir force between a nanosphere and a planar substrate.

The theory of the Casimir effect between a sphere and a planar surface beyond the Proximity Force Approximation has been investigated within alternative perspectives, including some developed by authors of the present work [34–40]. In this section we extend the formalism previously presented in Refs.[34,35] to calculate the finite-temperature Casimir force for the nanosphere-substrate setup displayed in Fig.(1), with respective dielectric functions, $\varepsilon_{ns}(\omega)$, and $\epsilon_{sub}(\mathbf{r},\omega)$. We evaluate, at first, the zero-temperature interaction energy as a sum over proper frequencies $\omega_k(\mathbf{r}_\perp;d)$ of the considered configuration:

$$\mathcal{E}(\mathbf{r}_\perp;d)=\frac{1}{2}\sum_r\hbar\omega_r(\mathbf{r}_\perp;d)-\frac{1}{2}\sum_r\hbar\omega_r(\mathbf{r}_\perp;d\to\infty). \tag{2}$$

Straightforward use of the Argument Principle method let us express the sum over proper mode frequencies as a sum over the zeros of a spectral function $G(\omega;\mathbf{r}_\perp;d)$ (discussed below). This is determined by the solutions of Maxwell equations with boundary conditions satisfied by the plate-sphere setup:

$$\mathcal{E}(\mathbf{r}_\perp;d)=\frac{1}{2\pi i}\oint_{\mathcal{C}}\frac{\hbar\omega}{2}\frac{\partial}{\partial\omega}\left[\log G(\omega;\mathbf{r}_\perp,d)-\log G(\omega;\mathbf{r}_\perp,d\to\infty)\right]d\omega. \tag{3}$$

Here, the contour $\mathcal{C}$ is defined along the imaginary axis of the complex ω plane and a semicircle in the right hand of this plane with its radius tending to infinity. The integral along the semicircle yields a null contribution, and the integral in (3) may be evaluated by considering a contour between $-i\infty$ to $i\infty$. By introducing the variable $\omega=i\xi$, an integration by parts leads to

$$\mathcal{E}(\mathbf{r}_\perp;d)=-\frac{\hbar}{4\pi}\int_{-\infty}^{\infty}\left[\log G(i\xi;\mathbf{r}_\perp,d)-\log G(i\xi;\mathbf{r}_\perp,\infty)\right]d\xi. \tag{4}$$

The Casimir force is then obtained by calculating the derivative $F(\mathbf{r}_\perp;d)=-\partial\mathcal{E}(\mathbf{r}_\perp;d)/\partial d$. The eigenfrequency set of the sphere-substrate setup $\{\omega_r(\mathbf{r}_\perp;d)\}$, is obtained by assuming that the vacuum fluctuations induce a charge distribution on the sphere, described at lowest level, as a dipole located at its center:

$$\mathbf{p}_{ns}^0=\alpha(\omega)\mathbf{E}^{vac}(\omega), \tag{5}$$

where $\alpha(\omega)=R^3(\epsilon_{ns}-1)/(\epsilon_{ns}+2)$ denotes the nanosphere polarizability. This dipole moment will induce in turn a charge distribution in the YBCO half-space. By using the images method it follows that the total induced dipole moment on the sphere is

$$\mathbf{p}_{ns}(\mathbf{r}_\perp)=\alpha(\omega)\left[\mathbf{E}^{vac}(\omega)+\mathbb{T}\cdot\mathbf{p}_{sub}(\mathbf{r}_\perp)\right]. \tag{6}$$

Here, $\mathbb{T}$ is the dipole-dipole interaction tensor $\mathbb{T}=(3\mathbf{rr}-r^2\mathbb{I})/r^5$, and $\mathbf{r}=(0,0,2(d+R))$ is a vector joining the centers of the sphere and the dipole charge distribution at a position $\mathbf{r}_\perp=(x,y)$ over the substrate surface. In turn, the relation between the dipole moment on the sphere and the dipole moment induced on the YBCO substrate is $\mathbf{p}_{sub}(\omega)=f_c(\omega;\mathbf{r}_\perp)\,\mathbb{M}\cdot\mathbf{p}_{ns}(\mathbf{r}_\perp)$, where $M=diag(-1,-1,1)$ is a diagonal matrix, and the contrast factor $f_c(\omega)\equiv(1-\epsilon_{sub}(\omega))/(1+\epsilon_{sub}(\omega))$. By substituting $\mathbf{p}_{sub}(\omega)$ into Eq.(6), we obtain a secular equation

$$\left[\alpha^{-1}(\omega)\mathbb{I}+f_c(\omega)\mathbb{M}\cdot\mathbb{T}\right]\cdot\mathbf{p}_{ns}(\omega)=\mathbf{E}^{vac}(\omega), \tag{7}$$

Preprints (www.preprints.org) | NOT PEER-REVIEWED | Posted: 6 December 2023 doi:10.20944/preprints202312.0293.v1

which, by introducing the function $u(\omega) = [1 - \epsilon_{ns}(\omega)]^{-1}$ and explicitly substituting $\alpha(\omega)$, may be re-expressed as the secular equation:

$$[-u(\omega)\mathbb{I} + \mathbb{H}] \cdot \mathbf{p}_{ns}(\omega) = \widetilde{\mathbf{E}}^{vac}(\omega), \tag{8}$$

where $\mathbb{H} = (1/3)[\mathbb{I} + R^3 f_c(\omega)\mathbb{M} \cdot \mathbb{T}]$, and $\widetilde{\mathbf{E}}^{vac} = (1/3)R^3\mathbf{E}^{vac}$. By performing the change of variable $\omega \to i\xi$ it follows that the matrix $\mathbb{H}$ in (8) is real; therefore, we may find a unitary transformation $\mathbb{U}$ such that $\mathbb{U}^{-1}\mathbb{H}\mathbb{U} = \lambda_r$, where λ_r are the eigenvalues of $\mathbb{H}$. This allows to introduce the spectral function

$$G(i\xi, d) \equiv \prod_r [-u(i\xi) + \lambda_r(i\xi, d)] = 0, \tag{9}$$

which in the present case implies three eigenvalues,

$$\lambda_{1,2}(i\xi, d) = \frac{1}{3}\left[1 + \frac{f_c(i\xi)}{[2(1 + d/R)]^3}\right]; \quad \lambda_3(i\xi, d) = \frac{1}{3}\left[1 + \frac{2f_c(i\xi)}{[2(1 + d/R)]^3}\right],$$

whose structure reflects the dipole-dipole interaction described by the tensor $\mathbb{T}$. Substitution of $G(i\xi, d)$ into Eq. (3) conduces to a final expression for Casimir force at null temperature:

$$\begin{aligned} F(d) &= \frac{\hbar}{4\pi}\frac{\partial}{\partial d}\sum_r \int_{-\infty}^{\infty} \log[-u(i\xi) + \lambda_r(i\xi, d)]\, d\xi \\ &= \frac{\hbar}{16\pi R}\frac{1}{(1 + d/R)^4}\int_{-\infty}^{\infty}\left[\frac{f_c(i\xi)}{-u(i\xi) + \lambda_1(i\xi, d)} + \frac{f_c(i\xi)}{-u(i\xi) + \lambda_3(i\xi, d)}\right] d\xi, \end{aligned} \tag{10}$$

where the fact that $\lambda_1(i\xi, d) = \lambda_2(i\xi, d)$ has been considered. This result may be generalized to the finite-temperature regime by use of the Matsubara formalism. In this approach, the frequency integration is replaced by a summation over discrete frequencies $\xi_n = 2\pi k_B T n/\hbar$, with n an integer number. In that case, the final expression for temperature-dependent Casimir force is:

$$F(d/R, T) = \frac{k_B T}{4R}\frac{1}{(1 + d/R)^4}\sum_{n=0}^{\infty}{}' \left[\frac{f_c(i\xi_n)}{-u(i\xi_n) + \lambda_1(i\xi_n)} + \frac{f_c(i\xi_n)}{-u(i\xi_n) + \lambda_3(i\xi_n)}\right], \tag{11}$$

where the prime implies that the $n = 0$ term should be multiplied by a factor $1/2$. We observe that the force scales as $F \sim 1/R$, so that this is maximized by the use of smaller nanospheres.

In the former expressions the functions $u(\omega)$ and $f_c(\omega)$ are respectively determined by the dielectric response of the nanosphere, ε_{ns}, and the planar substrate, ε_{sub}. The dielectric properties of the gold nanosphere may be simply represented by a Drude function $\varepsilon_{ns}(\omega) = 1 - \omega_{Au}^2/(\omega^2 + i\gamma_{Au}\omega)$, where the gold plasma frequency, $\omega_{Au} = 9.1$ eV, and the inverse scattering rate, $\gamma_{Au} = 0.02$ eV. Therefore, $u(i\xi) = -(\xi^2 + \gamma_{Au}\xi)/\omega_{Au}^2$. On the other hand, the dielectric response of the YBCO substrate requires a more elaborated discussion, which we present in the following section.

2.2. Ginzburg-Landau theory and the optical response of the YBCO substrate.

To characterize the dielectric response of the YBCO substrate we must determine the way in which the CP number density, $n_s(\mathbf{r})$, is spatially distributed under the action of the external magnetic field. With that purpose, we put forth a straightforward reformulation of the GL theory that explicitly incorporates two particular features of cuprates, like YBCO: i) a layered crystallographic structure in which superfluid transport of Cooper-like pairs (CPs) occurs along CuO_2 planes; ii) an extremely short CP coherence length, such that the GL parameter $\kappa \gg 1$. This latter property implies that charge carriers in these materials define constitute a weakly-interacting gas of strongly-bound pairs satisfying a Bose-Einstein statistics. These facts allow the description of SC charge transport in HTSCs as a 2D superfluid of Cooper-like pairs.

Preprints (www.preprints.org) | NOT PEER-REVIEWED | Posted: 6 December 2023 doi:10.20944/preprints202312.0293.v1

In the GL theory, the transit to the SC state is described as a second-order phase transition determined by a complex order parameter, $\Psi = |\Psi|e^{i\theta}$, null in the normal phase, but finite in the SC phase, characterizing a long-range order specified by the number density of SC pairs. In this theory the SC free energy per unit volume in presence of an external magnetic field is given by

$$f_s(T) = f_n(T) + a_T|\Psi|^2 + \frac{b}{2}|\Psi|^4 + \frac{1}{2m^*}\left(-i\hbar\nabla - e^*\mathbf{A}\right)^2\Psi + \frac{1}{2\mu_0}\mathbf{B^2}(\mathbf{r}), \tag{12}$$

where $f_n(T)$ is the normal state contribution, $e^* = 2m$ and $m^* = 2m$ are the charge and mass of CPs, while the parameters, $a_T = a_0(T - T_c)$ and $b > 0$, in the standard GL approach. The last term in (12) accounts for the electromagnetic energy of the field $B(\mathbf{r}) = \nabla \times \mathbf{A}(\mathbf{r})$. After the original GL proposal, Gorkov was able to derive the GL theory from the microscopic BCS theory for temperatures nearby T_c and, furthermore, made the identification $|\Psi|^2 = n_s$. A fundamental assumption in Gorkov's derivation is that the London condition $\kappa \gg 1$ holds; this is satisfied by type-I SCs only in the immediate neighborhood of T_c, whereas in the case of type-II SCs it has a wider region of applicability.

The total energy in the SC state, is obtained by spatial integration of Eq.(12), $\int f_s(T)d^3r$. It follows that the functional differentiation $\delta F_s(T)/\delta\Psi^*(\mathbf{r})$ leads to the non-linear GL differential equation:

$$\frac{1}{2m^*}\left(-i\hbar\nabla - \frac{e^*}{c}\mathbf{A}\right)^2\Psi + \left(a_T + b|\Psi|^2\right)\Psi, \tag{13}$$

while the differentiation $\delta F_s(T)/\delta\mathbf{A}(\mathbf{r})$ yields the current density

$$\mathbf{J}_s = -\frac{i\hbar(2e)}{2m^*}\left(\Psi^*\nabla\Psi - \Psi\nabla\Psi^*\right) - \frac{(2e)^2}{m^*}\mathbf{A}. \tag{14}$$

In absence of external fields or material boundaries, Eq.(13) predicts a homogeneous bulk ordering characterized by $n_s = |\Psi_\infty|^2 = -a_T/b$, for $a_T < 0$, whereas $|\Psi_\infty|^2 = 0$, for $a_T > 0$. On the other hand, for the case of a planar interface separating a normal metal ($x < 0$) and the superconductor ($x > 0$), with no magnetic field, the order parameter $\Psi(x) = \Psi_\infty \tanh[x/\sqrt{2}\xi(T)]$, where the GL correlation length $\xi(T) \equiv \left(\hbar^2/2m^*|a_T|\right)^{1/2}$, connecting a_T with the measured value of the CP coherence length.

On these terms, the optical response of HTSCs is characterized by considering a variant of the Ginzburg-Landau (GL) theory of superconductivity that takes into account the aforementioned properties of these materials. This is attained by the Lawrence-Doniach (LD) model, in which layered SC materials are described as a stacked array of 2D superconductors, coupled together by Josephson tunneling between adjacent layers [**?**]. Then, the order parameter in layer n, subject to the action of a vector potential $(\mathbf{A}, A_z)$, satisfies the equation:

$$-\frac{\hbar^2}{2m_{ab}}\left[\nabla_\perp - \frac{2ie}{\hbar c}\mathbf{A}\right]^2 - \frac{\hbar^2}{2m_c s^2}\nabla_n^2\psi_n + a_T\psi_n + b|\psi_n|^2\psi_n, \tag{15}$$

where $\nabla_n^2\psi_n = \psi_{n+1}e^{-2ieA_z s/\hbar c} - 2\psi_n - \psi_{n-1}e^{2ieA_z s/\hbar c}$, and s is the interlayer distance. In the long-wavelength limit $\lambda \gg s$, so that the ratio $(\Psi_n - \Psi_{n+1})/s \to \partial\Psi/\partial z$. in that case, Eq.(15) reduces to an anisotropic GL equation

$$-\frac{\hbar^2}{2}\left(\nabla - \frac{2ie}{\hbar c}\mathbf{A}\right)\cdot\left(\frac{1}{m}\right)\cdot\left(\nabla - \frac{2ie}{\hbar c}\mathbf{A}\right)\Psi + \left(\alpha_T + b|\Psi|^2\right)\Psi = 0, \tag{16}$$

where the reciprocal mass tensor $(1/m) = \mathrm{diag}(1/m_{ab}, 1/m_{ab}, 1/m_c)$. The mass anisotropy induces in turn an anisotropic CP coherence length, which can be shown to satisfy the relation, $\xi_i^2(T) = \hbar^2/2m_i|\alpha_T|$, where i identifies a particular axis of the crystallographic cell [**?**].

Preprints (www.preprints.org) | NOT PEER-REVIEWED | Posted: 6 December 2023 doi:10.20944/preprints202312.0293.v1

The explicit expression of $\Psi(\mathbf{r})$ is now obtained by assuming that the magnetic field is directed along the z direction, coincident with the crystallographic c-axis, $\mathbf{B} = B\mathbf{e}_z$. Then, the vector potential in the Landau gauge, $\mathbf{A} = Bx\,\mathbf{e}_y$, and the GL equation becomes:

$$\frac{-\hbar^2}{2m^*}\left(\nabla_\perp - \frac{ie^*}{\hbar}Bx\mathbf{e}_y\right)^2\Psi - \left(a_T + b|\Psi|^2\right)\Psi = 0, \tag{17}$$

where $m^* = 2m_{ab}$. It was shown by Abrikosov [27] that Eq.(17) admits an analytic solution given by a Jacobi theta function:

$$\Psi(\tilde{x},\tilde{y}) = C\exp[-\frac{1}{2}\kappa^2\tilde{x}^2]\theta_3\left[1;\sqrt{2\pi}\,\kappa i(\tilde{x}+i\tilde{y})\right], \tag{18}$$

where $\tilde{x} = x/\lambda_{ab}$, $\tilde{y} = y/\lambda_{ab}$, and the ab-penetration length, $\lambda_{ab}(T) \sim (n_s^{2D}(\mathbf{0},T)/m_{ab})^{-1/2}$. Fig. (1) depicts the resulting contours of constant probability defined by $|\Psi(\tilde{\mathbf{r}})|^2$. We observe a lattice structure with square elementary cells with periods $\mathcal{L}_x = \mathcal{L}_y = \sqrt{2\pi}/\kappa$. By writing $\Psi(\tilde{\mathbf{r}}) = |\Psi(\tilde{\mathbf{r}})|e^{i\chi(\tilde{\mathbf{r}})}$ it follows that the GL current density is given by $\mathbf{J}_s = (\hbar e/m_{ab})|\Psi|^2(\nabla\chi - (2e/\hbar c)\mathbf{A})$. In that case, the super-current lines coincide with the equi-probability contours, and the vortex cores are located at the darkest zones of the figure. Notice that the vortex size can be tuned by the substrate temperature T_{sub} which modulates the lattice parameter. In normal units, it follows that $\mathsf{L}_x(T) = \sqrt{2\pi}\xi_{ab}(T)$, so that $\mathsf{L}_x(2\,\mathrm{K}) \approx 6$ nm, whereas $\mathsf{L}_x(90\,\mathrm{K}) \approx 100$ nm [28].

2.3. Thermal properties of the order parameter.

The thermal properties of the order parameter can be determined by considering that cuprate superconductors exhibit a layered structure in which transport of strongly-bound CPs occurs mainly along double CuO_2 planes -the ab-planes- perpendicular to the c-axis. CPs displace along the ab and c directions with effective masses $m_{ab} \ll m_c$ [41]. Together with the condition $\kappa \gg 1$, this is indicative of a strongly binding pair interaction, leading the formation of a 2D weakly-interacting Bose gas, able to form a BEC [42]. In the low-momentum limit, the energy spectrum of the system can be expressed as a phonon dispersion relation, $\mathcal{E}_k \approx \hbar c_s k$, with c_s the sound's speed. This linear relation is consistent with Landau's criterion for superfluid transport [43]. In that case, the pair occupancy number can be expressed, for $T < T_c$, in the form

$$n^{2D}(\mathbf{r},T) = n_0^{2D}(\mathbf{r},T) + \sum_{\mathbf{k}>0}\frac{1}{\exp\left(\hbar c_s k/k_B T\right) - 1}. \tag{19}$$

By evaluating this latter expression and taking into account that in the dilute regime the density of superfluid charge carriers coincides with the condensate: $n_s^{2D}(\mathbf{r},T) \approx n_0^{2D}(\mathbf{r},T)$, it then follows that [44,45]

$$n_s^{2D}(\mathbf{r},T) = \left(1 - T^2/T_c^2\right)N|\Psi(\mathbf{r})|^2. \tag{20}$$

Here, $T_c = \left(2\pi\hbar^2 c_s^2 n^{2D}/k_B^2\zeta(2)\right)^{1/2}$ [44], where $\zeta(2)$ is a Riemann's zeta function , $\int d^2r|\Psi(\mathbf{r})|^2 = 1$, and N is the total number of charge carriers

2.4. YBCO dielectric response

The optical properties of HTSCs have been experimentally investigated for different compounds at several temperatures and frequencies using reflectivity and impedance-type measurements [47–49]. In particular, the dielectric function of YBCO samples has been measured, in the absence of an applied magnetic field, in the normal and SC states at $T = 100$ K and $T = 2$ K, respectively. For $T > T_c$, an

Preprints (www.preprints.org) | NOT PEER-REVIEWED | Posted: 6 December 2023 doi:10.20944/preprints202312.0293.v1

accurate representation of the dielectric response includes Drude, mid-infrared (MIR) intra-band, and phonon contributions:

$$\varepsilon_n(\omega) = \varepsilon_\infty - \frac{\omega_p^2}{\omega^2 + i\gamma(T)\omega} - \frac{\Omega_{mir}^2}{\omega^2 - \omega_{mir}^2 + i\Gamma_{mir}\omega} - \sum_{r=1}^{N_{ph}} \frac{\omega_{pr}^2}{\omega^2 - \omega_r^2 + i\gamma_r\omega}. \tag{21}$$

Here, $\varepsilon_\infty = 3.8$, the plasma frequency, $\omega_p(100\text{K}) = 0.75$ eV, and the inverse scattering rate $\gamma(T) = 0.037 + \gamma_1 T$ eV, with $\gamma_1 = 8 \times 10^{-15}$ eV/K. For the higher frequency contributions, the MIR parameters $\Omega_{mir} = 2.6$ eV, $\omega_{mir} = 0.26$ eV, $\Gamma_{mir} = 1$ eV, whereas the phonon parameters are given in SI. In the SC state, dissipative scattering does not occur, so that $\gamma \to 0$. In that limit, $(\omega \pm i\gamma_0)^{-1} \to \mathcal{P}\,(1/\omega) \mp i\pi\delta(\omega)$, and the dielectric function becomes:

$$\begin{aligned}\varepsilon_s(\omega; \mathbf{r}_\perp) = \varepsilon_\infty &- \left[\frac{i\pi\omega_p^2}{2\omega}\delta(\omega) + \frac{\omega_p^2}{\omega^2}\right]\left(1 - \frac{T^2}{T_c^2}\right)|\Psi(\mathbf{r}_\perp)|^2 - \frac{\omega_p^2}{\omega^2 + i\gamma(T)\omega}\left(\frac{T^2}{T_c^2}\right) \\ &- \frac{\Omega_{mir}^2}{\omega^2 - \omega_{mir}^2 + i\Gamma_{mir}\omega} - \sum_{r=1}^{N_{ph}} \frac{\Omega_{ir}^2}{\omega^2 - \omega_r^2 + i\gamma_r\omega}.\end{aligned} \tag{22}$$

In this case is also given by $\omega_p(2\text{K}) = 0.75$ eV, while the parameters ε_∞, Ω_{mir}, ω_{mir}, Γ_{mir} and the phonon parameters are very similar to those obtained in the normal situation. The fact that $\omega_{ps}(2\text{K}) = \omega_n(100\text{K})$ indicates that the dielectric response of this system is consistent with London's two-fluid model of superconductivity . In this scheme, the nanosphere and substrate permittivities are respectively given by $\varepsilon_{ns}(\omega) = \varepsilon_{Au}(\omega)$, $\varepsilon_{sub}(\omega, \mathbf{r}, T) = \varepsilon_{ab}^{(n)}(\omega, \mathbf{r}, T > T_c)$ and $\varepsilon_{sub}(\omega, \mathbf{r}, T) = \varepsilon_{ab}^{(s)}(\omega, \mathbf{r}, T < T_c)$.

3. Results

We show in Figure 2 the structure of Casimir force at $T = 2$ K, as function of the position of the Au nanosphere over the AL. Here, the nanosphere radius $R = \mathsf{L}_x(2\text{K}) \approx 4$ nm, and $d = 2R$. This figure reveals that the Casimir force displays a periodic structure congruent with the spatial charge distribution induced by the AL. I can be observed that the modulation amplitude $\Delta F = |F_{max} - F_{min}|$ is maximized at regions corresponding to the vortex cores, consistently with the fact that the material reflectivity is strongly reduced at these zones. In order to compare how these results are altered with increasing temperature, we present in Figure 3 a cross-section of the Casimir force surface at a fixed value of $\mathsf{L}_x = 0.5$, for three different temperatures: $T = 2$ K, $T = 40$ K, and $T = 90$ K, with corresponding lattice size: $L_x(2\text{K}) = 4.1$ nm, $L_x(40\text{K}) = 4.6$ nm, and $L_x(90\text{K}) = 16.4$ nm. We observe that in the low-temperature regime, $2 \leq T \leq 40$ K, very similar periodic patterns arise, essentially independent of the temperature, with a relatively small modulation amplitude $\Delta F \sim 0.04$ pN. On the other hand, for $T \approx T_c$ the vortex cell size increases, but the force modulation is drastically reduced.

Preprints (www.preprints.org) | NOT PEER-REVIEWED | Posted: 6 December 2023 doi:10.20944/preprints202312.0293.v1

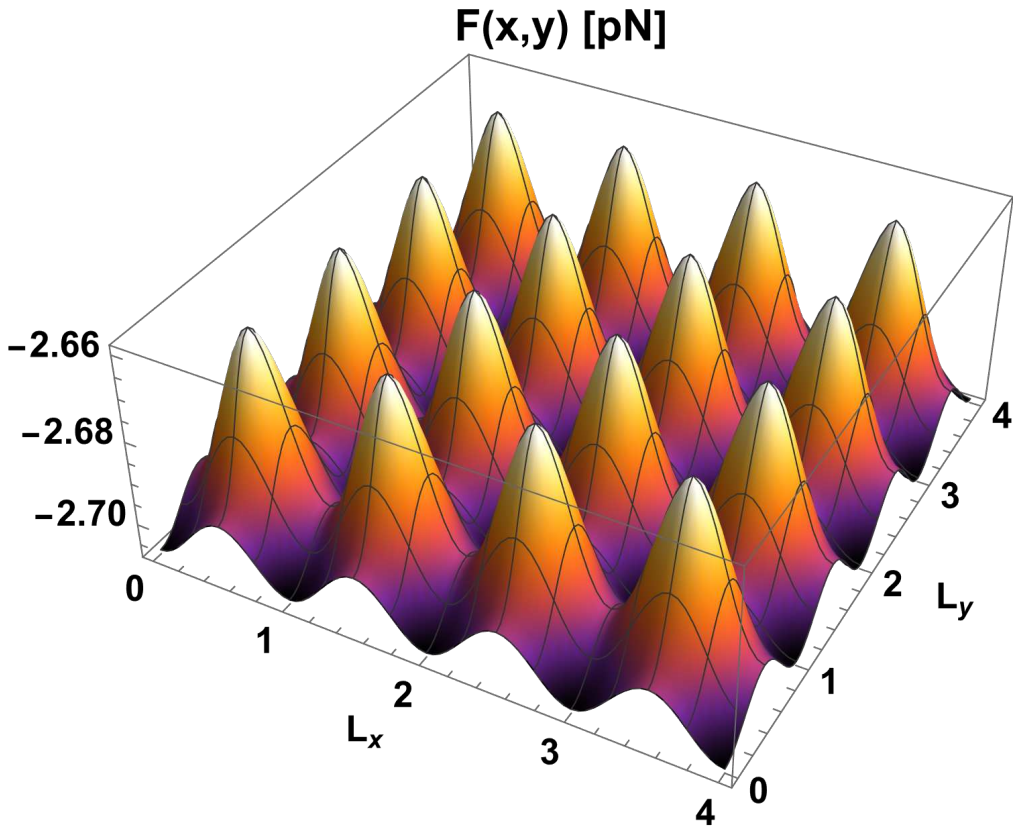

Figure 2. Periodic structure of the Casimir force as a function of the location of the Au nanosphere over the Abrikosov lattice at $T = 2$ K, for a fixed distance $d = 2R$. Here, $R = \mathsf{L}_x(2\,\mathrm{K}) \approx 4$ nm. It can be observed that the minimal strength of the Casimir force corresponds to the vortex cores.

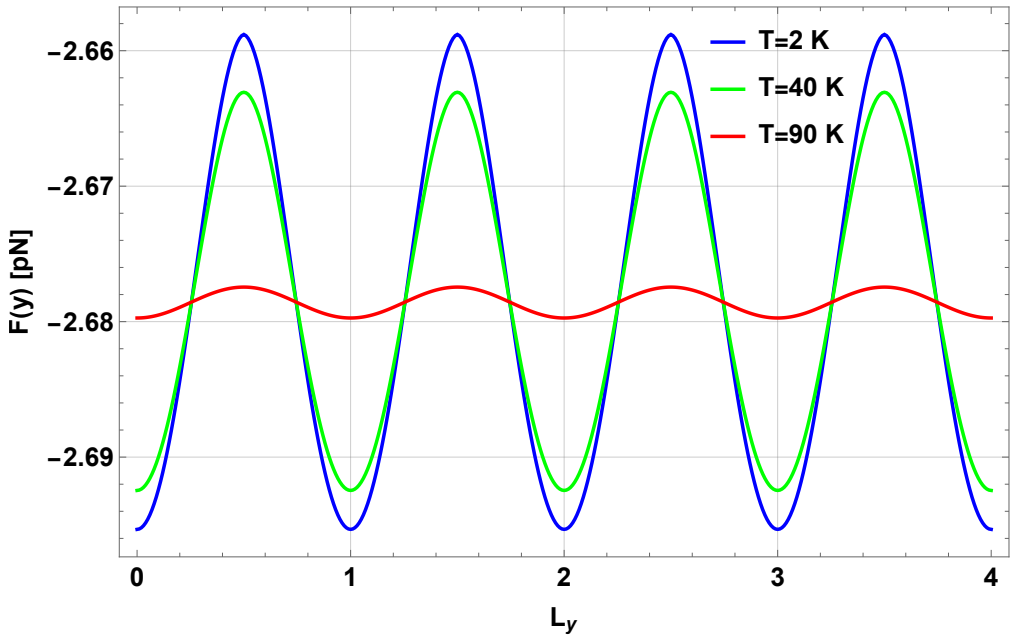

Figure 3. Comparison of the Casimir force profiles as a function of L_y, for a fixed value of $\mathsf{L}_x = .5n$ (with n integer), and $d = 2R$, at three different temperatures: i) $T = 2$ K, ii) $T = 40$ K, iii) $T = 90$ K. We observe that in the low-temperature regime the force magnitude shows almost coincident values up to $T = 40$ K, consistent with expectations that vacuum fluctuations overwhelm thermal fluctuations at nanometer separations.

 doi:10.20944/preprints202312.0293.v1

4. Discussion

The former results have been derived within a mean-field approach that neglects thermal fluctuations of the order parameter and pinning disorder. However, in the weak-interacting limit of Cooper pairs the effect of thermal fluctuations can be addressed through a perturbation expansion resulting from the evaluation of the functional integral $\mathcal{Z} = \int \mathcal{D}[\Psi]\mathcal{D}\Psi^* e^{-\beta F[\Psi]}$ [29], with $F_s[\Psi]$ given by the spatial integration of Eq.(12). The effect of disorder can be introduced by adding a white noise to the coefficients of the GL free energy and performing the $\mathcal{Z}$ functional integration, or by performing vortex matter simulations based on the numerical analysis of the time-dependent GL formulation [29,30].

Although the present work was focused on the action of strong magnetic fields $H \leq H_{c2}$, the effect of weak magnetic fields $H \geq H_{c1}$ can be straightforwardly discussed within the clean-limit of the London theory [28]. In that case, the order parameter is given by $|\Phi(r)|^2 \approx (1 + 2\xi_{ab}^2/r^2)^{-1}$, while the local magnetic induction $B(r) = \left[\Phi_0/2\pi\lambda_{ab}^2\right] K_0(\sqrt{r^2 + 2\xi_{ab}^2}/\lambda_{ab})$, where $K_0(x)$ is a modified Bessel function. Then the total order parameter can be built as product $\phi(\mathbf{r}) = \prod_i \phi_i(|\mathbf{r} - \mathbf{r}_i|)$, where $\mathbf{r}_i$ denotes the localization of the different vortexes, whereas the total magnetic induction $\mathbf{B}(\mathbf{r}) = \sum_i \mathbf{B}_i(|\mathbf{r} - \mathbf{r}_i|)$ [50].

In conclusion, we presented a general methodology aimed to evaluate the Casimir force in setups constituted by SC materials under the action of an external magnetic field. We have shown that the Abrikosov vortex lattice displayed by a type II superconductor induces Casimir forces with a periodic structure that mirrors the local charge redistribution due to superconducting currents conducing to magnetic fluxon confinement within the vortex cores. This approach may be applied to SC systems under different conditions of temperature, oxygen doping, and magnetic field configurations, allowing the analysis of alternative orderings competing with vortex matter, such as charge density waves [51], or the investigation of normal matter inside the vortexes subject to multiple Andreev reflections [52].

Author Contributions: Conceptualization, Shunashi Castillo-López, Raúl Esquivel-Sirvent, Giuseppe Pirruccio and Carlos Villarreal; Formal analysis, Shunashi Castillo-López, Raúl Esquivel-Sirvent, Giuseppe Pirruccio and Carlos Villarreal; Methodology, Shunashi Castillo-López, Raúl Esquivel-Sirvent, Giuseppe Pirruccio and Carlos Villarreal; Software, Shunashi Castillo-López and Carlos Villarreal; Writing – original draft, Shunashi Castillo-López, Raúl Esquivel-Sirvent, Giuseppe Pirruccio and Carlos Villarreal; Writing – review & editing, Shunashi Castillo-López, Raúl Esquivel-Sirvent, Giuseppe Pirruccio and Carlos Villarreal.

Funding: G.P. acknowledges financial support from UNAM DGAPA PAPIIT Grant No. IN104522, UNAM DGAPA PAPIME PE101223 and CONACyT Projects No. 1564464 and No. 1098652. R. E-S acknowledges partial support from CONACyT Project No. A1-S-10537.

Conflicts of Interest: The authors declare no conflict of interest.

References

1. H. B. G. Casimir, *Proc. K. Ned. Akad. Wet. B* **51**, 793 (1948).
2. E. M. Lifshitz, *Sov. Phys. JETP* **2**, 73 (1956).
3. S. K. Lamoreaux, *Phys. Rev. Lett.* **78**, 5 (1997).
4. B. W. Harris, F. Chen and U. Mohideen, *Phys. Rev. A* **62**, 052109 (2000).
5. G. Bressi, G. Carugno, R. Onofrio and G. Ruoso, *Phys. Rev. Lett.* **88**, 041804 (2002).
6. R. S. Decca, D. López, E. Fischbach and D. E. Krause, *Phys. Rev. Lett.* **91**, 050402 (2003).
7. F. Chen, G. L. Klimchitskaya, U. Mohideen and V. M. Mostepanenko, *Phys. Rev. A* **69**, 022117 (2004).
8. R. S. Decca, D. López, E. Fischbach, G. L. Klimchitskaya, D. E. Krause and V. M. Mostepanenko, *Annals of Physics (N. Y.)* **318**, 37 (2005).
9. D. E. Krause, R. S. Decca, D. Lopez and E. Fischbach, *Phys. Rev. Lett.* **98**, 050403 (2007).
10. G. Jourdan, A. Lambrecht, F. Comin and J. Chevrier, *Europhys. Lett.* **85**, 31001 (2009).
11. C. C. Chang, A. A. Banishev, R. Castillo-Garza, G. L. Klimchitskaya, V. M. Mostepanenko and U. Mohideen, *Phys. Rev. B* **85**, 165443 (2012).

12. A. A. Banishev, G. L. Klimchitskaya, V. M. Mostepanenko and U. Mohideen, *Phys. Rev. Lett.* **110**, 137401 (2013).
13. R. Castillo-Garza, J. Xu, G. L. Klimchitskaya, V. M. Mostepanenko and U. Mohideen, *Phys. Rev. B* **88**, 075402 (2013).
14. M. Bordag, G. L. Klimchitskaya, U. Mohideen and V. M. Mostepanenko, *Advances in the Casimir Effect* (Oxford University Press, 2009).
15. G. L. Klimchitskaya, U. Mohideen and V. M. Mostepanenko, *Rev. Mod. Phys.* **81**, 1827 (2009).
16. A. W. Rodriguez, F. Capasso and S. Johnson, *Nat. Phot.* **5**, 211 (2011).
17. G. L. Klimchitskaya, U. Mohideen and V. M. Mostepanenko, *Int. J. Mod. Phys. B* **25**, 171 (2011).
18. G. Bimonte, E. Calloni, G. Esposito, L. Milano and L. Rosa, *Phys. Rev. Lett.* **94**, 180402 (2005).
19. G. Bimonte, D. Born, E. Calloni, G. Esposito, E. Il'ichev, L. Rosa, O. Scaldaferri, F. Tafuri, R. Vaglio and U. Hübner, *J. Phys. A: Math. Gen.* **39**, 6153 (2006).
20. G. Bimonte, E. Calloni, G. Esposito and L. Rosa, *J. Phys. A: Math. Gen.* **39**, 6161 (2006).
21. G. Bimonte, D. Born, E. Calloni, G. Esposito, U. Hübner, E. Il'ichev, L. Rosa, O. Scaldaferri, F. Tafuri and R. Vaglio, *J. Phys. A: Math. Theor.* **41**, 164023 (2008).
22. G. Bimonte, *Phys. Rev. A* **78**, 062101 (2008).
23. R. A. Norte, M. Forsch, A. Wallucks, I. Marinkovic and S. Groblacher, *Phys. Rev. Lett.* **121**, 030405 (2018).
24. G. Bimonte, *Phys. Rev. A* **99**, 062101 (2019).
25. C. Villarreal and S.F. Caballero-Benítez, *Phys. Rev. A* **100**, 042504 (2019).
26. S. G. Castillo, López, R. Esquivel,ÄêSirvent, G. Pirruccio, and C. Villarreal *Sci. Reports* **12**, 2905 (2022). Castillo22
27. A.A. Abrikosov, *Rev. Mod. Phys.* **76**, 975 (2004).
28. J.F. Annett, *Superconductivity, Superfluids and Condensates*, Oxford University Press, Oxford (2004).
29. B. Rosenstein and D. Li, *Rev. Mod. Phys* **82**, 109 (2010)
30. G. Blatter et al., *Rev. Mod. Phys.* **66**, 1125 (1994)
31. W.-K. Kwok et al., *Rep. Prog. Phys.* **79**, 116501 (2016)
32. H. Suderow, I. Guillamón, J. G. Rodrigo, and S. Vieira, *Supercond. Sci. Tech.* **27**, 063001 (2014).
33. J. E. Sonier, J. H. Brewer, and R. F. Kiefl, *Rev. Mod. Phys.* **72**, 769 (2000).
34. C. Noguez, C. E. Román-Velázquez, R. Esquivel-Sirvent and C. Villarreal, *Eur. Phys. Lett.* **67**, 191 (2004).
35. C. E. Román-Velázquez, C. Noguez, C. Villarreal, and R. Esquivel-Sirvent, *Phys. Rev. A* **69**, 042109 (2004).
36. P. A. Maia Neto, A. Lambrecht and S. Reynaud, *Phys. Rev. A* **78**, 012115 (2008), doi:10.1103/PhysRevA.78.012115.
37. A. Canaguier-Durand, P. A. Maia Neto, I. Cavero-Peláez, A. Lambrecht and S. Reynaud, *Phys. Rev. Lett.* **102**, 230404 (2009), doi: 10.1103/PhysRevLett.102.230404.
38. M. Bordag, G.L. Klimchitskaya, U. Mohideen and V.M. Mostepanenko, *The Casimir Force Between Objects of Arbitrary Shape*, in Advances in the Casimir Effect, Oxford University Press (2009).
39. A. Canaguier-Durand, P. A. Maia Neto, A. Lambrecht and S. Reynaud, *Phys. Rev. Lett.* **104**, 0404003 (2010), doi: 10.1103/PhysRevLett.104.040403.
40. G. Bimonte, *Eur. Lett.* **118**, 20002 (2017), doi: 0.1209/0295-5075/118/20002.
41. M. Tinkham, *Introduction to superconductivity*, (Courier Corporation, 2004).
42. P. Nozieres and S. Schmitt-Rink, *J. Low Temp. Phys.* **59**, 195 (1985).
43. L. D. Landau and E. M. Lifshitz, *Statistical Physics: Volume 5*, (Elsevier, 2013).
44. S. Fujita and S. Godoy, *Quantum statistical theory of superconductivity* (Springer Science and Business Media, 1996).
45. M. Lomnitz, C. Villarreal, and M. De Llano,*Int. J. Mod. Phys. B* **27**, 1347001 (2013).
46. Y. Zuev, M. S. Kim, and T. R. Lemberger, *Phys. Rev. Lett.* **95**, 137002 (2005).
47. D. A. Bonn, A. H. O'Reilly, J. E. Greedan, C. V. Stager, T. Timusk, K. Kamaras and D. B. Tanner, *Phys. Rev. B* **37**, 1574 (1988).
48. T. Timusk, S. L. Herr, K. Kamaras, C. D. Porter, D. B. Tanner, D. A. Bonn, J. D. Garrett, C. V. Stager, J. E. Greedan and M. Reedyk, *Phys. Rev. B* **38**, 6683 (1988).
49. D. N. Basov and T. Timusk, *Rev. Mod. Phys.* **77**, 721 (2005).
50. E. H. Brandt, *Reports on Progress in Physics*, **58**, 1465 (1995).

 doi:10.20944/preprints202312.0293.v1

51. J. Chang *et al.*, *Nature Phys.* **8**, 871 (2012).
52. R. P. Huebener, *J. Supercond. Nov. Mag.* **32**, 475 (2019).